Journal of Power Sources 180 (2008) 704–710

Contents lists available at ScienceDirect

Journal of Power Sources

journal homepage: www.elsevier.com/locate/jpowsour

Oxidation failure modes of anode-supported solid oxide fuel cells

D. Sarantaridis*, R.A. Rudkin, A. Atkinson

Department of Materials, Imperial College London, Exhibition Road, London SW7 2AZ, UK

ARTICLE INFO

Article history:
Received 14 January 2008
Received in revised form 8 February 2008
Accepted 1 March 2008
Available online 14 March 2008

Keywords:
SOFC
Anode
Nickel
Oxidation
Redox
Fracture

ABSTRACT

Investigations on anode-supported solid oxide fuel cells (SOFCs) using Ni-based anode supports are presented aiming at understanding how much oxidation such a cell can tolerate before incurring irreversible mechanical damage. The cells were oxidised both directly in air and electrochemically. The different oxidation procedures performed exhibited different damage modes. For free-standing cells oxidised in air, the main damage mode was electrolyte cracking after oxidation of approximately 50% of the Ni in the substrate. However, cells oxidised electrochemically failed by substrate cracking after only ca. 5% of the Ni was oxidised, mainly due to the non-uniform nature of oxidation in the SOFC. Models of the stress generation and fracture processes were developed for interpretation of the results.

1. Introduction

As solid oxide fuel cell (SOFC) technology advances and comes closer to commercialization, durability related issues are of particular research interest. Of the different designs developed, the anode-supported cells (ASC) yield very good electrochemical performance, as they usually incorporate a Ni-YSZ substrate and anode, and a very thin (e.g. 10 μm) YSZ electrolyte, minimizing ohmic losses [1]. However, the redox (reduction–oxidation) instability of Ni cermets poses a major durability issue for Ni-based SOFCs, as described in detail in a recent review [2]. The ASC design, in particular, exhibits poor redox tolerance, both in experimental investigations and modelling studies [2], as its structural component is a thick (from a few hundred microns to greater than a millimetre) Ni-YSZ substrate. Although several redox studies have emerged recently, monitoring and analysis of the redox behaviour on a cell level is far from complete. Understanding of how much oxidation ASCs can tolerate before incurring irreversible mechanical damage is of great importance.

One issue that arises in carrying out practical redox cycling tests on cells and stacks is the way in which the oxidation is performed, and how a correlation between degree of oxidation and its effect can be extracted. For example, some investigators simply cut-off the fuel supply and disconnect the external electrical circuit during a cell test, allowing the anode to oxidise by adventitious leakage, whereas others pass air into the anode compartment. In general these methods do not allow the degree of oxidation to be simultaneously monitored. Waldbillig et al. [3] have attempted to estimate and control the degree of oxidation in tests by using a slow flow of air to the anode and measuring the depleted oxygen content of the anode exhaust stream. The situation is somewhat simpler when investigating the redox behaviour of free-standing samples, as the degree of oxidation can easily be determined by weight measurements [4].

Here, along with redox measurements on free-standing ASCs we have also oxidised cells electrochemically, achieving greater control over the degree of oxidation. Furthermore, this kind of oxidation is similar to failure due to fuel starvation (over-utilisation of fuel), thus providing useful information for a mechanism for which results have not been published in the open literature. Results on the relationship between degree of oxidation and mechanical failure are presented. The analysis involves post mortem observations and implementation of mechanical models for the interpretation of the failure modes.

2. Experimental

2.1. Samples

The redox investigations were performed on ASCs (anode substrate: 56 wt.% NiO/44 wt.% 8YSZ, electrolyte: 8YSZ, cathode: LSM/8YSZ) provided by Forschungszentrum Jülich, Germany. Cells

* Corresponding author. Present address: Department of Chemistry, University College London, 20 Gordon Street, London WC1H 0AJ, UK. Tel.: +44 20 7679 4528; fax: +44 20 7679 7463.
E-mail address: d.sarantaridis@ucl.ac.uk (D. Sarantaridis).

0378-7753/$ – see front matter © 2008 Elsevier B.V. All rights reserved.
doi:10.1016/j.jpowsour.2008.03.011

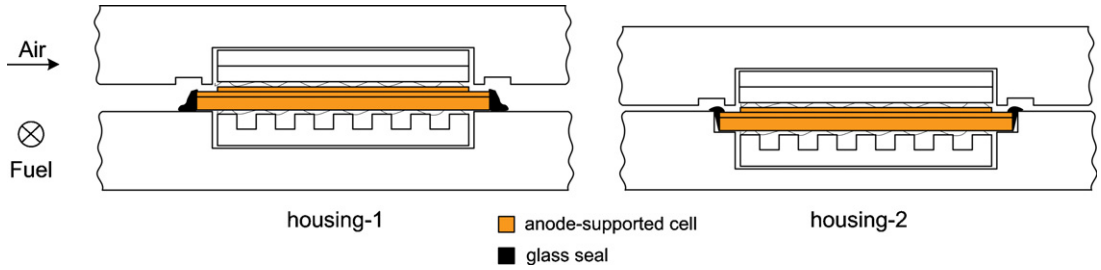

Fig. 1. Cross-section schematics of the two cell housing configurations used for electrochemical experiments.

of 50 mm × 50 mm × 1.5 mm dimensions (40 mm × 40 mm active area) were used for the electrochemical experiments. Specimens (ca. 25 mm × 10 mm × 1.5 mm) cut with a diamond saw from whole cells were used for free-standing oxidation experiments. The latter were cut such that every sample had a part of its area where no cathode was covering the electrolyte so that cracking of the electrolyte could be observed. The strength and fracture toughness measurements of the Ni-YSZ substrate in the reduced state were performed on bars of 50 mm × 5 mm × 1.5 mm cut from substrate plates. The plates were pre-treated under the same conditions as would be used for co-sintering an electrolyte layer so that they were in the same state as they would be in a typical ASC.

2.2. Electrochemical cell testing configuration

For the electrochemical experiments on the ASCs, a metal cell test housing was used. The metal employed was Alloy MA956 [5], which is a ferritic stainless steel. Annealing of the housing components at 900 °C for 1 h in air was performed in order to grow an electrically insulating alumina layer on the metal surfaces. Two different ways of supporting the ASCs were implemented (Fig. 1); one in which the anode substrate was sitting freely on the upper surface of the fuel plate (housing-1) and an other in which the cell was placed on a manufactured "step" at the fuel plate surface (housing-2), in order to achieve better gas sealing. In both cases the cell was sealed at its periphery (on the anode substrate side) to the fuel plate using a glass seal (mix of 50 wt.% dielectric encapsulant Du Pont 8190 and 50 wt.% Heraeus IP 041). For the current collection a fine Pt mesh (1250 squares cm^{-2} and 0.075 mm diameter) overlaid with a coarse mesh (256 squares cm^{-2} and 0.09 mm diameter) was used on both the anode and cathode sides. The fuel and air supplies were in a cross-flow arrangement. When in operation, an extra mass of 3 kg (~200 g cm^{-2} of active area) was applied on the air plate. The fuel (wet hydrogen/nitrogen mixtures or just wet hydrogen, see later for details) and air feeds to the cell during testing were supplied using an integrated computer-controlled mass flow and humidifier Fideris system (FC Power). Both fuel and air streams were preheated at ca. 220 °C before entering the high temperature environment (800–900 °C) of the furnace where the cell was held. Typical flow rates during the tests were in the range 500–1000 ml min^{-1}. Finally, the electrochemical testing was performed with the aid of an Autolab Potentiostat-Galvanostat (PGSTAT30), 10 Amp Booster (BST7217) and the accompanying software.

2.3. Redox procedures

The initial reduction procedure of the ASCs in the cell housing was as follows: heating up in nitrogen (flow rate 1 l min^{-1}) at 1 K min^{-1} to 900 °C and then introduction of 20% H_2/N_2 at a flow rate of 1 l min^{-1}. The hydrogen concentration was then gradually increased for 2 h (by 10 percentage points every 30 min until it reached 50% H_2/N_2) and then switched to only wet hydrogen (9 mol.% steam) at 300–500 ml min^{-1}. The cell was maintained at open-circuit voltage (OCV) for at least 3 h after the start of reduction. Throughout the procedure the air flow to the cathode was in the range 200–700 ml min^{-1}. The reduction of the small cells and bars was performed by inserting them in a tube furnace and maintaining a 10% H_2/N_2 atmosphere while heating up to 900 °C at 1 K min^{-1}, holding for 3 h and cooling at 1 K min^{-1}.

After a cell was reduced and its electrochemical performance recorded, the fuel flow was stopped, any applied load removed and the OCV was recorded. A known current (0.1–1 A) was then drawn for a specific time (20–300 s) and the OCV was again measured. This was repeated in successive steps until the cell failed. In this way the oxidation was achieved by electrochemically "pumping" oxygen through the electrolyte to the anode side. For the free-standing samples oxidation was performed at 800 °C (in a box furnace with ambient air) in steps, with cooling to RT (room temperature) after each step. A step consisted of inserting the sample directly from RT into the furnace (800 °C), allowing it to oxidise for a few seconds or minutes, and then taking out and letting it cool freely to RT. The degree of oxidation was determined after each step by the change in weight.

2.4. Strength and toughness measurements

The mechanical failure analysis required data for the strength and fracture toughness of the reduced Ni-YSZ substrate. These were obtained by using the 4-point bending technique (equipment Tinnius Olsen H20K-C) at room temperature and following the procedures described in the respective standard publications [6,7]. 12 specimens were used for the strength and 4 for the fracture toughness measurements. The four points of contact were made with rollers of 4 mm diameter, with a distance between the inner loading points of 11 mm, and 22 mm between the outer loading points. The sample and rollers were sandwiched between two metal blocks and a push rod applied the load on a bearing ball (with a flat face) that was sitting on the top metal block.

3. Results and discussion

3.1. Electrochemical oxidation of cells

The electrochemical oxidation of the cermet can be represented by

$$Ni + O^{2-} \rightarrow NiO + 2e^{-} \quad (1)$$

After the fuel shut down, and once the gaseous fuel remaining in the anode compartment has been oxidised, the cell's OCV will be governed by the equilibrium of the reaction:

$$Ni + \tfrac{1}{2}O_2 \rightleftharpoons NiO \quad (2)$$

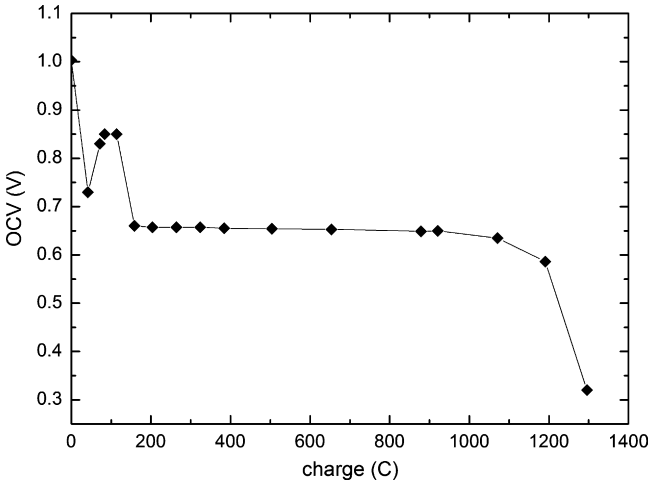

Fig. 2. OCV as a function of charge for electrochemical oxidation of an anode-supported cell at 850 °C.

The theoretical OCV is given by the Nernst equation:

$$\mathrm{OCV} = \frac{RT}{4F} \ln \frac{P_{O_2}^{\mathrm{cathode}}}{P_{O_2}^{\mathrm{anode}}} \quad (3)$$

where R is the universal gas constant, T the temperature (K), F the Faraday constant and P_{O_2} the oxygen partial pressure in the cell's cathode or anode side depending on the superscript. The chemical equilibrium constant K of Eq. (2) can on the other hand be described by the following equations:

$$K = \left(\frac{1}{P_{O_2}^{\mathrm{anode}}} \right)^{1/2} \quad (4)$$

$$K = \exp\left(-\frac{\Delta G^{\circ}}{RT} \right) \quad (5)$$

where ΔG° is the standard Gibbs free energy of formation of NiO. Using Eqs. (3)–(5), and thermodynamic data [8] for the temperature at which oxidation was performed, a theoretical value of 0.66 V was calculated for the corresponding OCV. Thus, the OCV should stabilise at 0.66 V when Ni and NiO are both present and close to equilibrium conditions in the anode side. According to Eq. (1) the amount of charge required for the total oxidation of the cell's anode substrate was estimated to be ca. 25,000 C. The effect of the anode layer to the total charge required for oxidation was neglected, the anode being only a few microns thick compared to the 1.5 mm thick anode substrate.

3.1.1. Housing-1 configuration

Fig. 2 shows a representative result of OCV evolution during electrochemical oxidation at 850 °C. The first stage of OCV drop (up to 150 C charge) is attributed to the consumption of most of the residual hydrogen in the fuel compartment. The establishment of the Ni/NiO equilibrium then follows as expected at the plateau OCV of 0.66 V. After passage of ca. 1100 C total charge the OCV is seen to deviate from the equilibrium value and drop rapidly after 1300 C. After this point it was observed that the air flow from the cathode side exhaust was greatly reduced—indicating a cracked cell. This was confirmed by the post-test examination (Fig. 3). The critical oxidation charge to cause cell fracture was estimated to be 1300 ± 100 C, representing oxidation of only ca. 5% of the Ni in the anode substrate. The disrupted cells displayed several wide radial cracks, mainly at the cell periphery, that ran through the substrate but did not extend to the cell's centre. The cathode surface showed

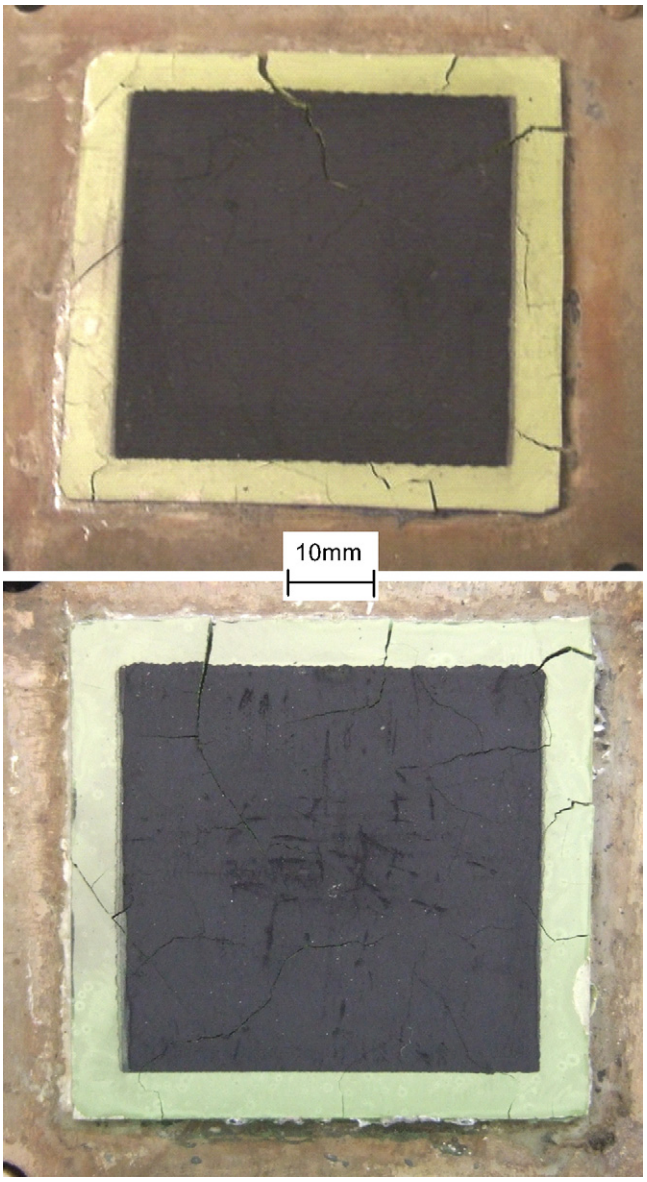

Fig. 3. Anode-supported cells (viewed from the cathode side) after failure by electrochemical oxidation in the housing-1 configuration.

marks produced by the Pt mesh, and indicated that the points with the best contact were mainly concentrated at the centre of the cell.

In order to check that the cracks observed at room temperature were not caused during cooling from the test temperature, an experiment was performed in which an ASC was sealed to the fuel plate in a thermal cycle (25–900–25 °C) at 1 K min^{-1}. After the cycle, the seal was found to have failed (cracked) but the cell was intact, leading to the conclusion that electrochemical oxidation caused the extensive cell cracking of Fig. 3.

3.1.2. Housing-2 configuration

Having established a value of 5% for the critical degree of electrochemical oxidation of the cells, the next experiment was performed to investigate if the cells can recover from a lower degree of oxidation. For this experiment the housing-2 configuration was used. Four (partial) redox cycles were performed on one ASC, with increasing degree of oxidation in each cycle, until the cell failed. Fig. 4a shows how the cell voltage behaved in each redox cycle, as the anode was electrochemically oxidised again by drawing cur-

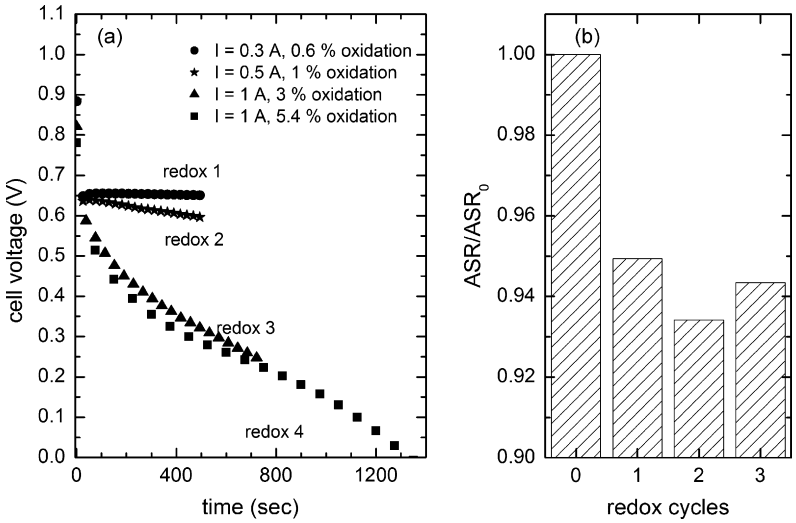

Fig. 4. (a) Cell voltage as a function of time and current drawn for four electrochemical partial redox cycles at 850 °C, each one corresponding to different degree of oxidation. (b) Cell's relative ASR (ASR_0 after initial reduction) at 850 °C as a function of the electrochemical partial redox cycles.

rent for specific time. It was found that for up to 3% oxidation the cell's performance could be recovered by subsequent reduction (the latter performed following the initial reduction procedure). It was noticed moreover that a non-destructive oxidation can even improve the cell's performance, as shown by the change in the area specific resistance (ASR, measured by the slope of the respective *I–V* curve between OCV and 0.7 V) (Fig. 4b). Other investigators have also observed improvement in performance after non-destructive redox cycling of SOFCs [9,10]. These observations suggest that some degree of redox may initially improve performance by conditioning the Ni network and enhancing conductivity. Nevertheless, after ca. 5% oxidation the OCV again fell to zero (Fig. 4a) and could not be restored by reduction with hydrogen, indicating a disrupted cell. Post mortem analysis this time revealed a rather different failure mode (Fig. 5). In addition to some cell cracking, buckling was also observed, apparently caused by the lateral edge restraint imposed by the different sealing geometry in housing-2.

3.2. Redox of free-standing small cells

Interrupted oxidation of the small free-standing samples of ASCs did not have the same effect as the electrochemical oxidation in the housing configurations. Even full oxidation of the samples did not result in any macroscopic effect other than the colour change of the cermet (grey when reduced and green when oxidised). Observation in the optical microscope however revealed cracking of the electrolyte and/or cathode (Fig. 6). The critical degree of oxidation to cause cracking of the electrolyte was estimated from these observations (four specimens) to be in the range 49–75%. These values correspond to the stage when cracks were distributed throughout the electrolyte surface and could easily be observed with the optical microscope. Therefore, possible earlier initiation of a small number of cracks with narrow openings could have occurred, but not been detected.

3.3. Interpretation of mechanical failure

Earlier analytical mechanical modelling [2,11], supported by more recent numerical studies [12], has concluded that the failure mode for an unconstrained and uniformly oxidised ASC should be by channel cracking of the electrolyte, predicting a critical substrate oxidation strain of 0.1–0.2%. The redox behaviour of the substrate used in the ASCs tested here has been reported previously [13]. On first oxidation, following an interrupted oxidation procedure, a linear relationship between expansion strain and degree of oxidation has been observed for the range of 20–90% oxidation (Fig. 7). Therefore, from the data of Fig. 7 and the modelling predictions, channel cracking is expected for a degree of oxidation above approximately

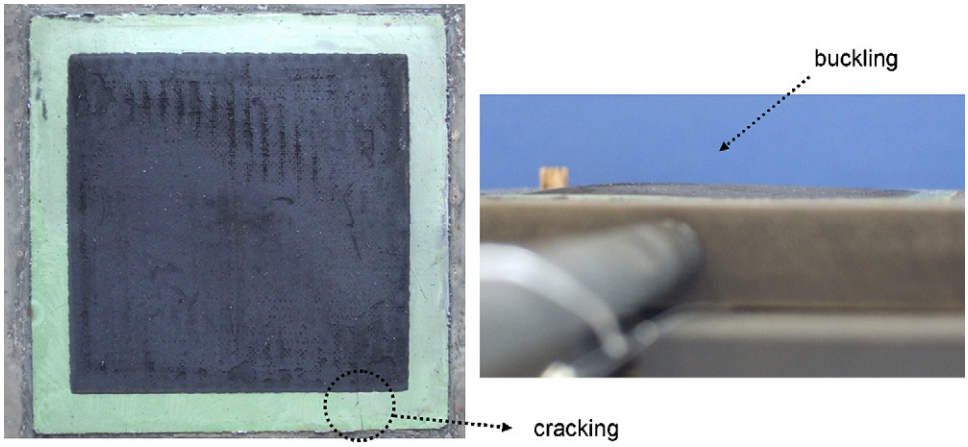

Fig. 5. Anode-supported cell (viewed from the cathode side (left) and fuel-inlet side (right)) after failure by electrochemical oxidation in the housing-2 configuration.

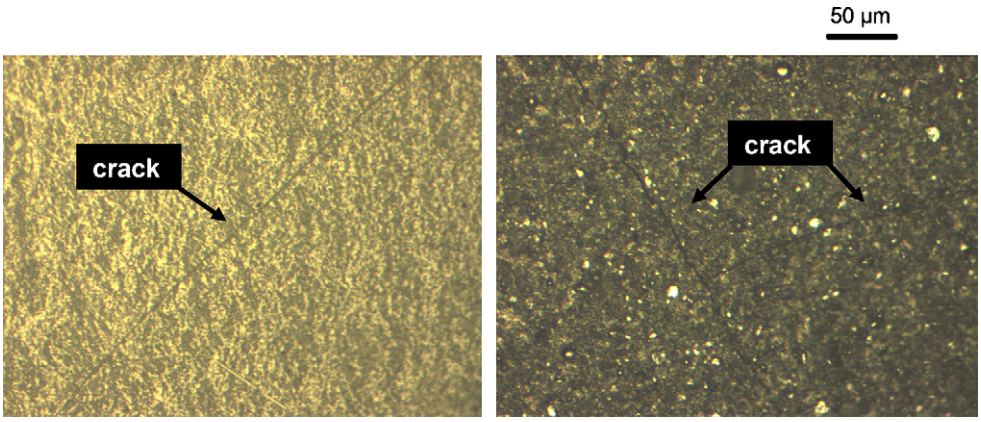

Fig. 6. Cracking of electrolyte (left) and cathode (right) in free-standing ASCs as detected in an optical microscope for 49–75% degree of oxidation (oxidation temperature 800 °C).

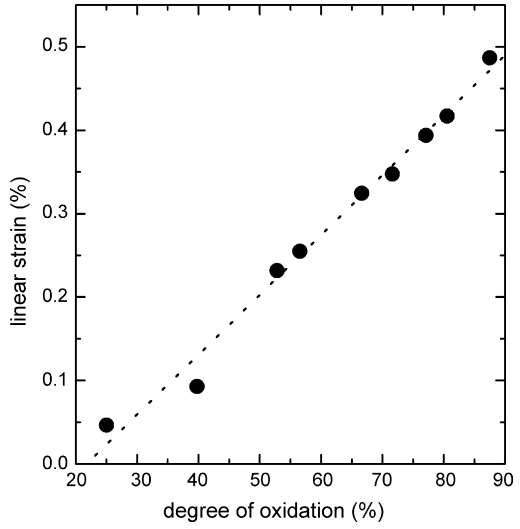

Fig. 7. Expansion strain of the cells' anode substrate in the range between 20 and 90% oxidation [13].

40–50%. This is slightly lower than the range 49–75% observed for the free-standing samples, but is in reasonable agreement considering uncertainties in critical mechanical properties and in detection of the initial stage of cracking. It should be noted, nonetheless, that the free-standing cells were also thermally cycled, due to the oxidation procedure followed and thus some thermal cycling fatigue may have also been involved. However, this is probably not a significant effect in our case, as cracking was detected for slightly higher degrees of oxidation than predicted.

In the electrochemical oxidation experiments, on the other hand, the critical extent of oxidation for failure was significantly lower, at approximately 5% (both housing-1 and -2 configurations) and by a different failure mode. At operating temperature the degree of edge constraint imposed by the glass sealant at the periphery of the ASC is not known. However, the particular glass used has a transition temperature of approximately 600 °C and therefore is likely to be soft and offer negligible constraint at the operating temperature in housing-1 configuration, unless the expansion due to oxidation is very rapid. In the housing-1 case complete failure of the anode substrate occurred, rather than failure of only the electrolyte. The cracks observed at the cell periphery have wide openings indicating that they are the result of tensile stresses and large displacements in this region (Fig. 3).

One way in which peripheral tensile stresses can be generated is if the oxidation is non-uniform and concentrated in the central part of the cell. This leads to a central zone of expansion that will create a radial compressive stress in the surrounding material and a tensile hoop (tangential) stress. Here we present a simple elastic model of this process based on assuming radial symmetry and a sharp boundary between a central oxidised zone and a surrounding un-oxidised zone (Fig. 8a). The solution to this problem can be found in standard mechanics textbooks, e.g. [14]. For the situation considered here the solution is

$$\frac{\sigma_\theta}{E_2 \varepsilon_{ox}} = \frac{1}{\beta}\left(\frac{r_1^2}{r_2^2} + \frac{r_1^2}{r^2}\right) \quad (6)$$

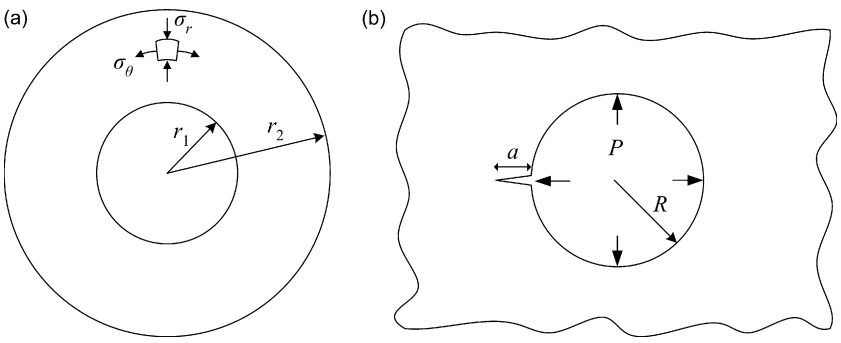

Fig. 8. Schematics of models for the case of non-uniform oxidation. (a) Stress–strain problem. The area with radius r_1 is oxidised and that between r_1 and r_2 is un-oxidised, σ_θ is the hoop stress and σ_r is the radial stress generated. (b) Fracture problem. An infinite plate with a crack of length a at the edge of a circular hole of radius R is subjected to an internal pressure P.

Table 1
Bending strength and fracture toughness values, including the respective standard deviation, of the Ni-YSZ substrate used

Number of samples	Bending strength (MPa)	Weibull modulus	Fracture toughness (MPa m$^{1/2}$)
12	108 ± 14	8.9	
4			2.2 ± 0.2

where

$$\beta = \frac{E_2}{E_1}\left(1-\frac{r_1^2}{r_2^2}\right)(1-\nu_1)+\left\{\left(1+\frac{r_1^2}{r_2^2}\right)+\nu_2\left(1-\frac{r_1^2}{r_2^2}\right)\right\} \quad (7)$$

and σ_θ is the hoop stress, E the elastic modulus, ε_{ox} the oxidation strain, ν the Poisson's ratio and r the radius. The subscript 1 refers to the oxidised region of radius $r < r_1$ and subscript 2 to the un-oxidised region $r_1 < r < r_2$. The maximum tensile stress occurs at the boundary between the oxidised and un-oxidised regions ($r = r_1$) and is of order $E_2\varepsilon_{ox}$. In the reduced state Young's modulus for the substrate has been measured to be approximately 32 GPa, whereas in the oxidised state it is higher at approximately 74 GPa [13]. Poisson's ratio is assumed to equal 0.3 for both the reduced and oxidised state, based on data from [15] and the fact that estimation of the hoop stress from Eqs. (6) and (7) is not particularly sensitive to its value. The bending strength of the substrate in the reduced state was found to be ca. 108 MPa (Table 1). Weibull analysis was also performed for an evaluation of the effect of sample volume on failure probability [16]. A Weibull modulus of $m = 8.9$ was estimated from the Weibull plot of flexural strength measured on the test specimens (Fig. 9). The failure probability F, for a stress σ_c that is characteristic of the stress distribution during cell oxidation (in our case the stress at the boundary of the oxidised region $r = r_1$), was calculated using the following equation:

$$F(\sigma_c) = 1 - \exp\left(-\frac{V_{eff}}{V_0}\left(\frac{\sigma_c}{\sigma_v}\right)^m\right) \quad (8)$$

where σ_v and V_0 are parameters derived from the bending strength measurements. The effective volume, V_{eff}, for the case of Fig. 8a is given by

$$V_{eff} = 2\pi h \int_{r_1}^{r_2} \frac{\left(\frac{r_1^2}{r_2^2}+\frac{r_1^2}{r^2}\right)^m}{\left(\frac{r_1^2}{r_2^2}+1\right)}\, r\,dr \quad (9)$$

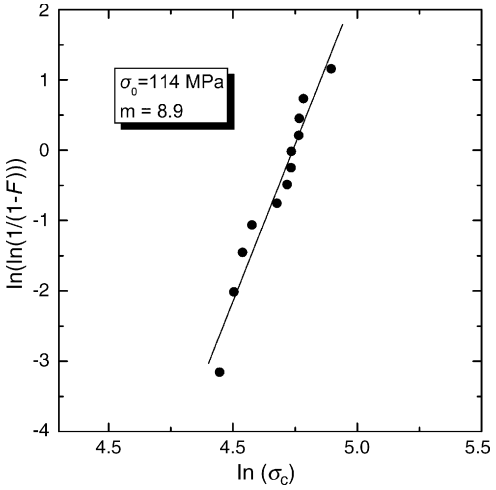

Fig. 9. Weibull plot of the flexural strength for the reduced substrate (Ni-YSZ), showing also the values of the Weibull parameters σ_0 and m.

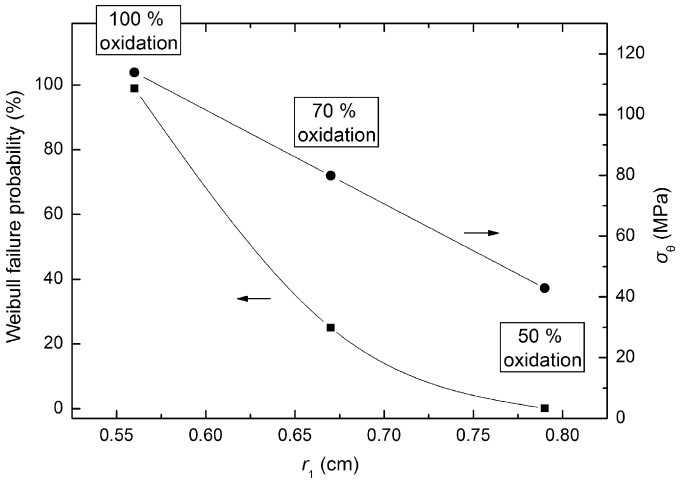

Fig. 10. Calculated hoop stress σ_θ generated at the border of an oxidised area of radius r_1, and the respective Weibull failure probability, for different degrees of oxidation occurring in the oxidised area, when it accommodates the 5% average oxidation distributed over $r_2 = 2.5$ cm.

where h is the thickness of the substrate. Although the mechanical properties are likely to be different at operating temperature, the room temperature values can nevertheless be used to form an initial assessment of the stress and likely damage induced by non-uniform oxidation, since the effect of temperature, on the mechanical properties of those SOFC materials for which data exist, is smaller than effects due to other variables (such as porosity or composition)[17].

The stresses generated in this problem depend on the area over which the oxidation is distributed (i.e. the value of r_1). The overall average measured 5% critical oxidation, when spread over different areas, corresponds to different degrees of oxidation within r_1 and hence different strains and stresses (which can be estimated using Fig. 7 and Eq. (6), respectively). Three cases of different degree of oxidation within r_1 were investigated – namely 100%, 70% and 50% – assuming $r_2 = 2.5$ cm and $r_1 = r_2/(\%\ \text{local oxidation}/\%\ \text{overall oxidation})^{1/2}$.

The results of the model are presented in Fig. 10. It is apparent that the larger the area the lower is the hoop stress caused by a given average amount of oxidation. If the average 5% oxidation is concentrated as 100% oxidation in a central region with $r_1 = 0.55$ cm, this will generate a hoop stress of 117 MPa at the border of oxidised and un-oxidised regions and a high probability (close to 100%) of causing damage of the type shown in Fig. 3. Conversely, if (for the same average 5% oxidation) the degree of oxidation in the central region is only 50%, then $r_1 = 0.79$ mm and the maximum stress is reduced to 42 MPa with a negligible probability of causing failure.

An alternative approach to analysing failure is using fracture mechanics. The stress intensity K_I for a radial crack of length a at the edge of a circular hole of radius R in an infinite plate under the action of an internal pressure P (which does not act on the faces of the crack) is known (Fig. 8b) [18]:

$$K_I = P\sqrt{\pi a}F_1 \quad (10)$$

where F_1 is a tabulated function of a/R. This can approximate the situation in Fig. 8a, with P being replaced by σ_θ at $R = r_1$. From Eqs. (6) and (7) and for $r_2 \to \infty$, the stresses for the infinite plate case can be calculated, and by using Eq. (10) the K_I profiles of the three cases of Fig. 10 as a function of crack length can be derived (Fig. 11). K_I rises rapidly with crack length and then reaches an approximate plateau which indicates that the crack will be unstable and grow rapidly once the stress intensity exceeds the fracture toughness K_{Ic}, measured to be ca. 2.2 MPa m$^{1/2}$ for the reduced substrate (Table 1).

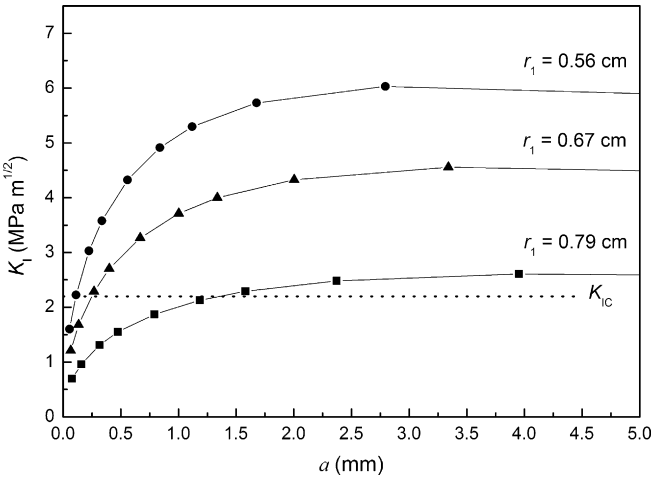

Fig. 11. Stress intensity K_I (modelling prediction) for a radial crack of length a at the edge of a circular hole under internal pressure in an infinite plate. The three cases correspond to those of Fig. 10 for $r_2 \to \infty$ and internal pressure equal to the respective hoop stress at r_1. K_{IC} is the fracture toughness measured for the Ni-YSZ substrate.

Again, as the oxidation area decreases and the local degree of oxidation increases, higher values for the stress intensity factor are obtained. It is observed that the toughness limit can be exceeded for an initial flaw length of 0.1 mm and above, depending on the area in which the overall average 5% oxidation is assumed to take place. Hence, fracture mechanics also shows that an average oxidation as low as 5% can be catastrophic for the ASC if the oxidation is not uniform. The non-uniform electrochemical oxidation is likely to have occurred in our case due to good electrode contact with the current collector meshes being preferentially in the central region of the cell.

In the housing-2 case different failure modes were observed but the critical degree of oxidation was again estimated to be ca. 5%. Although the fuel plate was designed to allow for a 1% oxidation strain of the cell support, post mortem investigation showed that the substrate's expansion was constrained and buckling was caused. It is very likely that the presence of the glass sealant, albeit in a "soft" state, decreased significantly any free space for the substrate's expansion. It is not clear at which stage of oxidation buckling occurred, as the observations were made only in the fully oxidised state and at room temperature after the experiment. A possible scenario is that, as with the housing-1 case, non-uniform oxidation took place initially, creating some cracking that in turn initiated an uncontrollable oxidation situation. The housing's geometric restrictions then prevented formation of wide cracks but deformed the cell as shown in Fig. 5.

One issue that arises in the above analyses, and in the estimation of degree of oxidation using Faraday's law, is the effect of electrolyte cracking. If during electrochemical oxidation the electrolyte cracks, oxidation will also occur due to air diffusion/flow from the cathode side, affecting the control of the oxidation process. It is assumed here that this does not play a significant role, as electrochemical oxidation was performed relatively quickly and electrolyte cracking is expected only for values of local degree of oxidation above 50%.

4. Conclusions

The redox behaviour of anode-supported cells was investigated with the objectives of determining the critical degree of oxidation to cause mechanical failure and of understanding the respective failure modes. Interrupted oxidation of free-standing cells resulted in failure by extensive electrolyte channel cracking at a critical degree of oxidation of ca. 50% in reasonable agreement with fracture mechanics analysis. Electrochemical oxidation, on the other hand, of cells incorporated in metal housings, led to fully disrupted cells (anode substrate also cracked) at only approximately 5% oxidation. For degrees of oxidation <5% in the metal housings, however, electrochemical performance could be recovered. When the cell was sealed into the housing so as to provide little edge constraint, the cracking patterns due to electrochemical oxidation were consistent with tensile cracking in the outer regions of the substrate driven by an oxidation-induced expansion of the inner region. A mechanical model of cell stability has been developed in which oxidation is assumed to occur preferentially within a central zone. Based on measurements of critical mechanical properties for the Ni-YSZ substrate used, both Weibull (fracture stress) and fracture mechanics analyses showed that a degree of oxidation as low as 5% can indeed be detrimental when only a small central region is oxidised. When the cell was sealed into the housing using a less deformable arrangement the cell was buckled after failure. However, the critical degree of oxidation to cause failure was again only approximately 5%, suggesting that the initial failure was again caused by preferential oxidation in a central zone.

In general it can be concluded that non-uniform oxidation processes will have more catastrophic effects than uniform ones, and are also likely to occur in other oxidation scenarios such as leaks in seals or at high fuel utilisation.

Acknowledgements

This work was carried out as part of the European Commission's Real-SOFC Project, contract no. SES6-CT-2003-502612. The authors also wish to thank Prof. Nigel Brandon for access to cell-testing facilities and colleagues at Forschungszentrum Jülich for provision of cells.

References

[1] R.N. Basu, G. Blass, H.P. Buchkremer, D. Stover, F. Tietz, E. Wessel, I.C. Vinke, J. Eur. Ceram. Soc. 25 (2005) 463–471.
[2] D. Sarantaridis, A. Atkinson, Fuel Cells 7 (2007) 246–258.
[3] D. Waldbillig, A. Wood, D.G. Ivey, J. Power Sources 145 (2005) 206–215.
[4] M. Ettler, G. Blaß, N.H. Menzler, Fuel Cells 7 (2007) 349–355.
[5] Special Metals Corporation, http://www.specialmetals.com/products/incoloyalloyma956.php.
[6] British Standard BS EN 658-3:2002.
[7] British Draft Standard DD CEN/TS 14425-5:2004.
[8] R.C. Weast (Ed.), CRC Handbook of Chemistry and Physics, 55th ed., CRC Press, Cleveland, 1974, p. D-47.
[9] R. Cunningham, R. Collins, G. Saunders, in: M. Mogensen (Ed.), Proceedings of the sixth European Solid Oxide Fuel Cell Forum, European Fuel Cell Forum, Lucerne, 2004, pp. 309–318.
[10] A. Schuler, V. Nerlich, in: U. Bossel (Ed.), Proceedings of the Fuel Cells for a Sustainable World, European Fuel Cell Forum, Lucerne, 2006, p. A061.
[11] D. Sarantaridis, A. Atkinson, in: U. Bossel (Ed.), Proceedings of the Seventh European SOFC Forum, European Fuel Cell Forum, Lucerne, 2006, p. P0768.
[12] J. Laurencin, G. Delette, M. Dupeux, F. Lefebvre-Joud, ECS Trans. 7 (2007) 677–686.
[13] D. Sarantaridis, R.J. Chater, A. Atkinson, J. Electrochem. Soc. 155 (2008) B467–B472.
[14] D.W.A. Rees, Mechanics of Solids and Structures, McGraw-Hill, London, 1990, p. 650.
[15] A. Selçuk, A. Atkinson, J. Eur. Ceram. Soc. 17 (1997) 1523–1532.
[16] D. Munz, T. Fett, Ceramics: Mechanical Properties, Failure Behaviour, Materials Selection, Springer-Verlag, Berlin, 1999, pp. 143–147.
[17] A. Atkinson, P. Bastid, Q. Liu, J. Am. Ceram. Soc. 90 (2007) 2489–2496.
[18] T. Fett, D. Munz, Stress Intensity Factors and Weight Functions, Computational Mechanics Publications, Southampton, 1997, p. 188.